Front. Chem. Sci. Eng. 2022, 16(6): 886–896
https://doi.org/10.1007/s11705-021-2125-z

RESEARCH ARTICLE

Chemical reactions of oily sludge catalyzed by iron oxide under supercritical water gasification condition

Houjun Zhang[1], Fang Chen[1], Jipeng Xu[1], Jinli Zhang[1], You Han (✉)[1,2]

1 School of Chemical Engineering and Technology, Tianjin University, Tianjin 300072, China
2 Tianjin Key Laboratory of Membrane Science and Desalination Technology, Tianjin University, Tianjin 300072, China

© Higher Education Press 2022

Abstract Supercritical water gasification is a promising technology in dealing with the degradation of hazardous waste, such as oily sludge, accompanied by the production of fuel gases. To evaluate the mechanism of Fe_2O_3 catalyst and the migration pathways of heteroatoms and to investigate the systems during the process, reactive force field molecular dynamics simulations are adopted. In terms of the catalytic mechanisms of Fe_2O_3, the surface lattice oxygen is consumed by small carbon fragments to produce CO and CO_2, improving the catalytic performance of the cluster due to more unsaturated coordination Fe sites exposed. Lattice oxygen combines with •H radicals to form water molecules, improving the catalytic performance. Furthermore, the pathway of asphaltene degradation was revealed at an atomic level, as well as products. Moreover, the adsorption of hydroxyl radical on the S atom caused breakage of the two C–S bonds in turn, forming •HSO intermediate, so that the organic S element was fixed into the inorganic liquid phase. The heteroatom O was removed under the effects of supercritical water. Heavy metal particles presented in the oily sludge, such as iron in association with Fe_2O_3 catalyst, helped accelerate the degradation of asphaltenes.

Keywords oily sludge, SCWG, ReaxFF, Fe_2O_3, heteroatoms

1 Introduction

Oily sludge (OS) [1,2], a kind of solid hazardous waste, is inevitable to be produced from crude oil during extraction, transportation, storage, and refining processes. Usually, OS is considered as a complex mixture of water–oil–solid, and its 30%–50% part is made up of crude oil [3,4]. Due to its exposure to the local environment, OS cannot be effectively handled, it causes environmental pollution, leading to the waste of resources. Therefore, finding an alternative method to recycle resources efficiently to avoid pollution becomes important.

Until now, various traditional and emerging technologies such as pyrolysis [1,5], biodegradation [2], extraction [6], and ultrasonication [7] have been employed in the resource utilization of OS and in the sustainable development of the environment. However, the shortcomings of the abovementioned methods are observed from the perspectives of operation conditions, equipment technical supports, and utilization efficiency. Most studies, while highlighting the conversion rate of the resources, ignore the treatment of the subsequent pollutants [4,8], owing to the presence of heteroatoms N, S and O in organic matters, such as asphaltene. Therefore, it is important to adopt an alternative way that considers two crucial options in treating OS. Supercritical water gasification (SCWG) technology takes advantage of the unique properties of supercritical water (SCW) [9–11] ($T_C \geqslant 647.15$ K; $P_C \geqslant 22.1$ MPa) to dispose of sludge effectively [12], and the pollutants produced by pyrolysis like sulfur oxides could not be formed in the SCWG process, as well as the elimination for the requirements of drying process. Adar et al. [13] investigated the effects of temperature, solid content, and catalyst addition on the sewage sludge gasification in SCW, and found detected no concentration of H_2S in the produced gas which contained fuel gases such as H_2 converted from sludge. Hantoko et al. [14] examined the potential of sludge to generate syngas in SCWG conditions with thermodynamic analysis and experiments, demonstrating advantages of the higher temperature and the lower concentration sludge for H_2-rich syngas. Notably, SCWG played an active role in the immobilization of heavy metals with reduced toxicity [15]. However, the high temperature is believed to be the

Received August 15, 2021; accepted September 30, 2021

E-mail: yhan@tju.edu.cn

main contributor to the corrosion of the reactor which brings higher costs [16]. The addition of catalysts contributes to moderate the extreme reaction conditions [17], enabling the realization of the equivalent yields of the products under mild conditions. Furthermore, Chen et al. [16] examined several commercial heterogeneous catalysts on the gasification reaction of sludge in near and SCW conditions with some factors. The gasification efficiency of degradation of organic matter was related to the amounts of the heterogeneous catalyst tightly. On the other hand, heterogeneous catalysts can be easily separated and recycled at the end of the reaction.

Due to the excellent oxygen storage capacity, oxygen carrier particles like Fe-, Ni-, and Cu-based materials have strong oxidation ability for adoption as a catalyst in the gasification process [18,19]. Moreover, the oxidation state is closely associated with gasification efficiency as it promotes higher degradation efficiency [18,20]. Fe_2O_3 is advantageous as it provides stable existence, has low cost, is environment friendly, and is usually employed as a catalyst in reactions. Herein, the adaptation of Fe_2O_3 as a catalyst is suitable for degrading organic matters in the SCWG process. It is experimentally difficult to explore the microscopic reaction mechanism with Fe_2O_3 and SCW due to the limitations of experimental detection methods and the harsh conditions. Therefore, exploring method to figure out the mechanism eventually can help exhibit the evolution of the intermediates in the system.

Recently, the reactive force field (ReaxFF) molecular dynamics simulation (MD) method proposed by van Duin et al. [21] has been employed as a powerful tool [22] to describe the bond formation and breakage with ReaxFF force field trained by density functional theory (DFT), which enables us to investigate the evolution of the intermediates during complex chemical reactions. Additionally, ReaxFF has the advantage of maintaining balance with the accuracy and acceptable computational cost in large-scale systems compared with quantum mechanics. Herein, amounts of works related to SCW conditions are studied via ReaxFF method. Zhang et al. [23] studied the degradation mechanism of coal and the hydrogen production in SCW through ReaxFF MD and reported that the H atom in SCW contributed to the cleavage of C–O and C–N bonds, and that the cleavage of the C–C bond induced by SCW enhanced the ring-opening efficiency. The heteroatom N was converted into NH_3 rather than NO_x at the end of the reaction. Han et al. [24] evaluated the synergistic effect between Fe_2O_3 catalyst and SCW in promoting the degradation of naphthalene (NAP) to generate CO and H_2 during the SCWG process, and also investigated the parameters, the amount of SCW molecules and concentration of NAP. Additionally, several studies have been published on the gasification of 2,4,6-trinitrotoluene [25], lignin [26], benzo[a]pyrene [27] and dibutyl phthalate [28] in SCW conditions using the ReaxFF MD method by our group.

In this work, asphaltene was chosen as a model component represented for OS, ReaxFF MD was performed to investigate the Fe_2O_3 catalytic performance of asphaltenes degradation during SCWG process. The simulation concentrated on the catalytic mechanism of Fe_2O_3 catalyst, fuel gases generation and the heteroatoms (e.g., S and O), migration mechanism by tracing and analyzing the trajectory at the atomic level. The effects of heavy metals were taken into consideration. The study attempts to shed light on the mechanism of Fe_2O_3 catalyst, providing a theoretical basis for the industrial application of the SCWG process with efficient catalysts.

2 Simulation method

Asphaltene, a complicated mixture mainly consisting of varieties of complex polymer hydrocarbons and their non-metallic derivatives, has already been investigated widely to figure out its molecular structure and some have been applied in MD simulations. The chosen asphaltene models, PA3 molecule structure [29,30], and the whole system are shown in Fig. 1. PA3 molecule structures analyzed by the combination of atomic force microscope and scanning tunnelling microscopy were selected to work as the model compounds shown in Fig. 1(a), the same as other simulation works. DFT calculations via Becke-3-Lee–Yang–Parr functional and a 6-311++G(d,p) basis set [31,32] were carried out by Gaussian 09 to obtain optimized asphaltene and H_2O molecules, iron oxide nanoparticle was constructed through bulk into sphere cluster with a dimeter of 2.5 nm. Likewise, Fe sphere cluster with the same dimeter of 0.6 nm was established through the same way. Thereafter, the modified Fe_2O_3 serving as catalyst was positioned in the center of the cubic cell with periodic boundary which was constructed by Amsterdam Modeling Suite software supplied by SCM Inc., surrounded by other reactant molecules distributed randomly shown in Fig. 1(b), and the details of each reaction systems are exhibited in Table 1. Systems 3, 4 and 5 investigate the effects of heteroatoms, and system 6 serves as the reference system.

A ReaxFF Fe/Cr/O/S developed by Shin et al. [33] was adopted to perform all simulations. Geometry optimization was essential to eliminate the possible simulation result errors caused by the unreasonable structure of the initial system for every system. Additionally, another function of geometry optimization was to optimize the Fe_2O_3 sphere cluster. Clearly, all simulations with periodic boundary were carried out under the conditions of NVT ensemble [28,34], employing Berendsen thermostat to controlling temperature with a damping constant of 100 fs. In addition, the time step of 0.25 fs was adopted [26], and then the temperature was heated up with a heating rate of 20 $K \cdot ps^{-1}$ from 0 to 300 K. Subsequently, an additional 10 ps simulation was performed under 300 K to further optimize

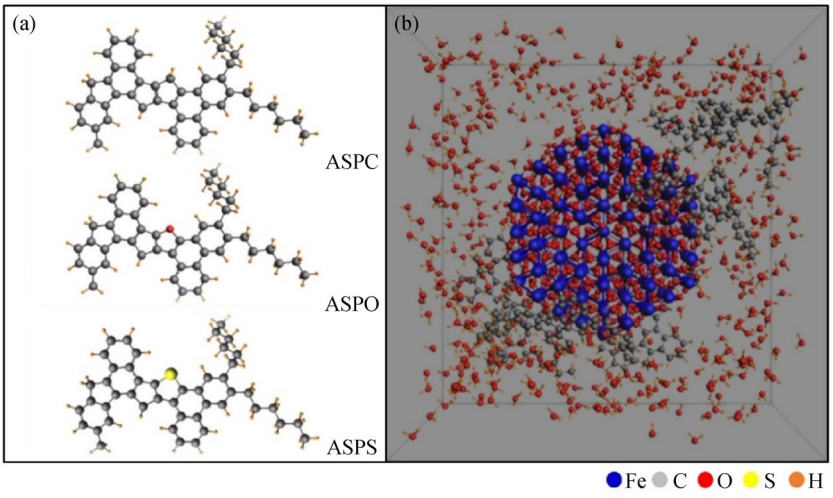

Fig. 1 (a) Structure of asphaltenes; (b) the initial structure of system. (ASPC refers to the asphaltene without heteroatoms modified, ASPO and ASPS refer to the asphaltene modified with the heteroatom O and S, respectively.)

Table 1 Details of the degradation systems

No.	Temperature/K	Catalyst	No. compound	No. H_2O	Time/ps	Density/(g·mL^{-1})
1	2300	Fe_2O_3	–	–	3000	0.76
2	2300	Fe_2O_3	–	500	3000	0.76
3	2300	Fe_2O_3	5 ASPC	500	3000	0.76
4	2300	Fe_2O_3	5 ASPO	500	3000	0.76
5	2300	Fe_2O_3	5 ASPS	500	3000	0.76
6	2300	–	5 ASPC	500	3000	0.76
7	2300	Fe_2O_3	5 ASPS	Reuse	3000	0.76
8	3000	Fe_2O_3	5 ASPS	500	3000	0.76
9	2300	Fe-Fe_2O_3	5 ASPC	500	3000	0.76
10	3000	Fe_2O_3	10 Thiophenes	500	3000	0.76

the system, which is consistent with the function of geometry optimization. Afterwards, the system temperature increased to a target value at a rate of 100 K·ps^{-1}, and was kept 3 ns for date collection finally. Most importantly, the trajectory was analyzed through ReaxFF module in AMS software.

Sorensen and Voter [35] pointed out that the initial reaction was kept compared with raising temperature to accelerate dynamic simulation, which is consistent with Arrhenius equation. Thereafter, raising temperature become a common strategy in ReaxFF dynamic simulations to saving computational cost without modifying the original reaction pathway. For example, Han et al. [24] investigated the degradation of NAP with Fe_2O_3 catalyst in SCW conditions at 3000 K using ReaxFF method. Wang et al. [36] studied carburization of C_2H_4 pyrolysis on Fe catalyst at 1500, 2000 and 2500 K with ReaxFF simulation, and found that the reaction path showed the similarity, only exhibiting the different reaction rates. Herein, to balance the computational cost and the reaction rate, 2300 K was chosen as the reaction temperature in this work (more details shown in Electronic Supplementary Material (ESM)).

In order to make a comprehension between the results of different systems, several equations are defined, which contain aromatic ring opening efficiency, carbonaceous products yield, and lattice oxygen contribution (LOC). All the formulas are listed as follows:

$$\text{Aromatic ring opening efficiency} = \frac{\text{number of opened aromatic rings}}{\text{total number of aromatic rings}} \times 100\%, \quad (1)$$

$$\text{Carbonaceous products yield} = \frac{\text{number of C atoms in products}}{\text{total number of C atoms in asphaltene}} \times 100\%, \quad (2)$$

$$\mathrm{LOC} = \frac{\text{lattice oxygen consumption}}{\text{total O atoms in cerbonaceous products}} \times 100\%. \quad (3)$$

3 Results and discussion

3.1 Mechanism of crystal morphology change of the Fe_2O_3 catalyst

Generally, the unsaturated coordination number of Fe active sites are related to the oxidation state of Fe-based catalysts closely, the lower the valance state of Fe is, the more surface-active sites of unsaturated coordination are, in other word, the higher the catalytic performance of the catalyst is. However, Fe_2O_3 catalyst adopted in gasification reaction has the highest conversion of reactants compared to other iron oxides [18]. Therefore, certain transformation of the crystal morphology exists during the process, which is of significance to understand the catalytic mechanism. By tracking the evolution of the Fe_2O_3 morphology changes, the relationship between the catalytic performance and the crystal morphology are revealed at atomic level.

In order to eliminate the misperception from the catalyst itself and the effects of SCW, systems 1 and 2 were carried out to exhibit the crystal morphology changes of Fe_2O_3 cluster in pyrolysis and SCW conditions, and the time evolution of crystal morphology changes and number of by-products molecules show in Figs. S1 and S2 (cf. ESM), respectively. Compared to the original, the crystal morphology still maintains the crystal structures, ignoring large amounts of hydroxyl groups adsorbed on Fe atoms in SCW condition. Meanwhile, the phenomenon of O_2 production shows consistently with the results that Fe_2O_3 cluster exhibits self-reduction at high temperature, while the number of O_2 molecules produced in SCW conditions are less than the case of pyrolysis, owing to the combination of H radicals generated from SCW catalyzed by Fe_2O_3 catalyst with the active lattice oxygen on the surface of Fe_2O_3 cluster, generating H_2O. Likewise, the absence of H_2 production has also been explained, but the consumption of lattice oxygen has little impact on the crystal morphology under this circumstance. Herein, the change of crystal morphology lies in the presence of reactants under SCWG condition.

Firstly, Fe_2O_3 cluster undergoes a surface reconstruction process in the initial stage of the reaction, as shown in Fig. 2. Free carbon fragments from asphaltene molecules get close gradually and adsorb on the catalyst surface through C–O bond, causing the dehydrogenation of the terminal hydroxyl. Then, the group adsorbed on the surface of the catalyst exhibits a reaction of reforming, adsorption formation turning into Fe–C rather than C–O bond, which makes two hydroxyls adsorbed on the C atom. Obviously, the structure of OH–C–OH formation is unstable and will be converted into other substances immediately, such as aldehydes and ketones. With the removal of H_2O molecule from the unstable group forming a ketone group, C atom would capture the active lattice oxygen of the surface subsequently and diffuses into the system to form CO_2 molecule through the cleavage of Fe–O bond finally. Moreover, small carbon fragments adsorbed on the surface of Fe_2O_3 cluster bonded with the active lattice oxygen produce not only CO_2 molecules, but also CO molecules in the similar path. In sum, the free carbon fragments bond with the active lattice oxygen on the surface of the Fe_2O_3 cluster generating small amounts of CO and CO_2 molecules in the initial stage of the reaction, causing more Fe active sites with unsaturated coordination to be exposed on the surface compared to the original, which accelerate the catalytic degradation of asphaltene molecules into small molecular compounds. Secondly, the formation of asphaltene molecule adsorbed on the surface with Fe–C bonds is transformed from vertical to parallel after the surface construction, and the aromatic ring becomes unstable to further convert into short straight chains or small molecules under the catalysis of Fe_2O_3 in the next period of time. Interestingly, the carbon fragments adsorbed on Fe sites could destroy the alignment of the surface to create vacancy defects, contributing to the C diffusion into the inside, which can be seen in Fig. 3. And Bentria et al. [37] investigated the carburization mechanisms from the surface to bulk of Fe, and found that the C atoms of carbide adsorbed on the surface diffused to the body, indicating the C atoms moved from a lower coordinated environment to a higher coordinated stage, which shows consistently with our results of catalyst carburization. Finally, Fig. 4 shows the migration of inside lattice oxygen into H_2O molecules, which does not mean that the inside lattice oxygen generates H_2O molecules only, and the generation of H_2O molecule is took an

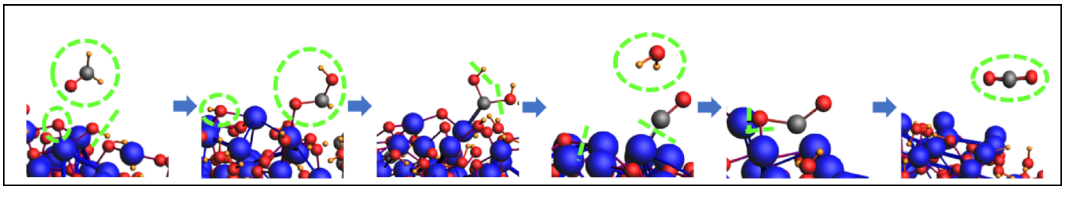

Fig. 2 Surface reconstruction of the Fe_2O_3 catalyst.

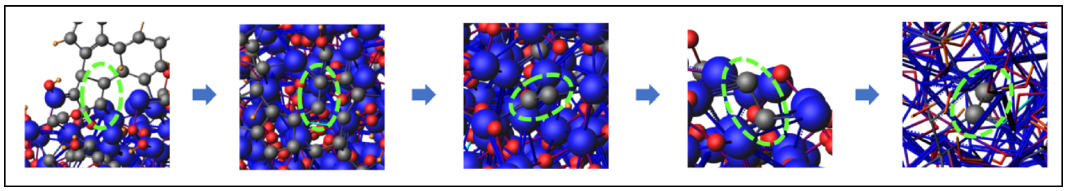

Fig. 3 Mechanism of catalyst carburization.

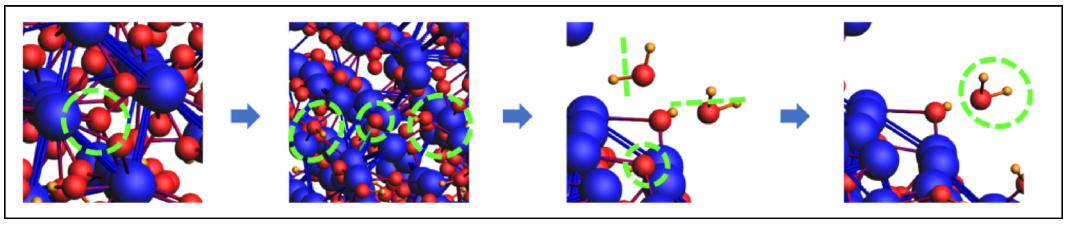

Fig. 4 Migration of lattice oxygen.

example to show the change of crystal morphology. The inside lattice oxygen migrates to the surface of the cluster under the effects of hydroxide radicals adsorbed on Fe atoms with Fe–O bonds, which are generated by SCW, and the carbon fragments. Subsequently, H radicals from SCW bond with the lattice oxygen to generate H_2O molecule, while the two hydroxide radicals adsorb on the Fe sites. It is obvious that the migration of lattice oxygen is confirmed in the Fe_2O_3 catalytic system during SCWG process. Accordingly, the three reactions mentioned above are the main reasons for the changes in the crystal morphology of the Fe_2O_3 catalyst, and the specific morphologies of fresh and used are shown in Fig. S3 (cf. ESM).

In general, the migration of Fe atoms in the cluster is considered to be the activation of the catalyst [38]. From the perspective of the structure of the nanoparticles, generally speaking, the edge atoms are more likely to obtain much higher kinetic energy than other atoms, turning into active sites in suit. Also, the activated atoms could move to the vacancy caused by the movement of another activated atom, due to the activated Fe atoms transferring kinetic energy to the rest of the Fe atoms, which finally forms the phenomenon. Meanwhile, the active sites promote the degradation of asphaltenes after adsorption. Combination with the morphology change of Fe_2O_3 cluster and the migration of the Fe atoms reveals the catalytic mechanism of Fe_2O_3 catalyst in details.

3.2 Evolution of asphaltene molecules into species of the system

3.2.1 Degradation pathway under catalytic condition

Owing to the difficulty in the degradation process of the stable structure of aromatic ring, to figure out the cleavage of aromatic ring is of significance in the degradation process of asphaltene. The mechanism of asphaltene molecules containing different heteroatoms shows the similarity through tracking the evolution of the asphaltene molecules. The degradation of different asphaltene molecules focused on the rupture of aromatic rings and the fracturing of the linkage of heteroatoms O/S in the molecules primarily, causing the molecular structure with the similar aromatic ring structure. Herein, the degradation process of asphaltene on Fe_2O_3 catalyst is obtained to reveal the mechanism at atomic level shown in Fig. 5.

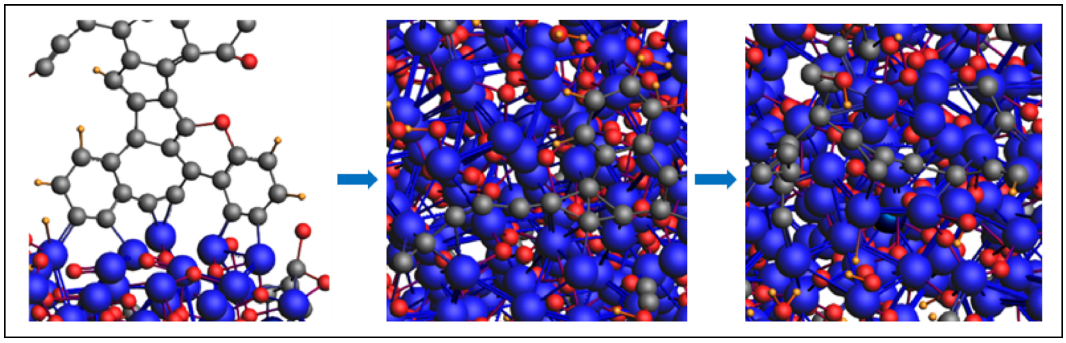

Fig. 5 Degradation path of asphaltene molecule during catalytic SCWG process.

Firstly, the asphaltene molecule is adsorbed on the surface of the Fe_2O_3 catalyst with H atoms captured by Fe_2O_3 cluster forming Fe–C bond, and the trend of phenomenon is rising swiftly after the consumption of the lattice oxygen on the surface. Subsequently, due to dehydrogenation and the combination of the influence of the SCW and catalyst, the aromatic ring becomes irregular, gradually leading to the destruction of the conjugated system, which could be transferred into linear carbon chain with small ring structures after ring opening and rearrangement reactions. Finally, the transferred structures gradually generate small molecule gas products with the simulations continuing.

Owing to different molecular structures in diverse asphaltene molecules, the degradation rate of asphaltene molecules is significantly vary from each other in the same Fe_2O_3 catalytic system, in spite of similar degradation mechanism. Herein, the aromatic ring opening efficiency and carbonaceous production yield are introduced to exhibit the difference, whose values are shown in Fig. 6. In general, the aromatic ring opening efficiency calculated by Eq. (1) is consistent in trend shown in Fig. 6(a), with rapidly increasing till 100% after a period of inefficient interval. Saturated coordination of Fe atom which works as the active sites for the degradation process is the major contributor to the period of the low catalytic activity, due to that the catalytic performance is relevant to the valance state of Fe-based catalysts closely. Herein, the phenomenon corresponds to the stage of the surface lattice oxygen captured by small carbon fragments, leading to rare adsorption of aromatic compounds, on the other hand, it is demonstrated that the low catalytic activity of Fe_2O_3 catalyst in the initial stage of the degradation process. And then, the degradation rate of all the systems with catalyst participation presents a rapid upward trend and the simulation time point when it starts to rise is different in different asphaltene systems, as a matter of fact, that is related to the conjugated structure of aromatic rings, which could make the molecular structure more stable. Moreover, the asphaltene molecules doped with heteroatoms are easier to break out at the heteroatoms, making the molecular structure smaller, in brief, the conjugated system of molecular structure is getting smaller, which leads to the degradation of the compound easier.

3.2.2 Product distribution

Generally, the solubility of organic compounds has been improved greatly in the SCW condition [11], and SCW works not only solvent but also reactant contributing to the higher gasification efficiency in the process of SCWG. The gasified products mainly consist of CO, CO_2, CH_4 and H_2 which could be used as syngas and raw materials to generate other important products. And the number of H_2O and gas products with time in different systems is shown in Fig. 7.

It can be seen clearly in Figs. 7(a) and 7(b) that the number of H_2O molecules and H_2 molecules present an exactly opposite trend in the whole process. On one hand, it is a remarkable fact that the catalytic ability of saturated Fe_2O_3 catalyst is relatively weak, so that the H_2O molecules could hardly be broken to generate •H and •OH radicals on the surface of Fe_2O_3. On the other hand, SCW, as a reactant, could supply •H radicals and •OH radicals that can participate in the reaction in oxidizing compounds, meanwhile, the •H radicals could bond with each other to generate H_2. However, the abundant lattice oxygen in Fe_2O_3 catalyst competes •H radicals with the pathway of generating H_2 to form H_2O. Therefore, the tendency of the number of H_2O and H_2 molecules without catalyst is differ from that with catalyst. The quantities of H_2 molecules in the later stage of the simulation demonstrate an ascending state that could be attributed to the reduction of Fe_2O_3 to FeO. Certainly, FeO has advantages in catalyzing hydrogen production compared Fe_2O_3 catalyst, so as to the contrary trend of H_2O and H_2 molecules in the later simulation process. Meanwhile, the

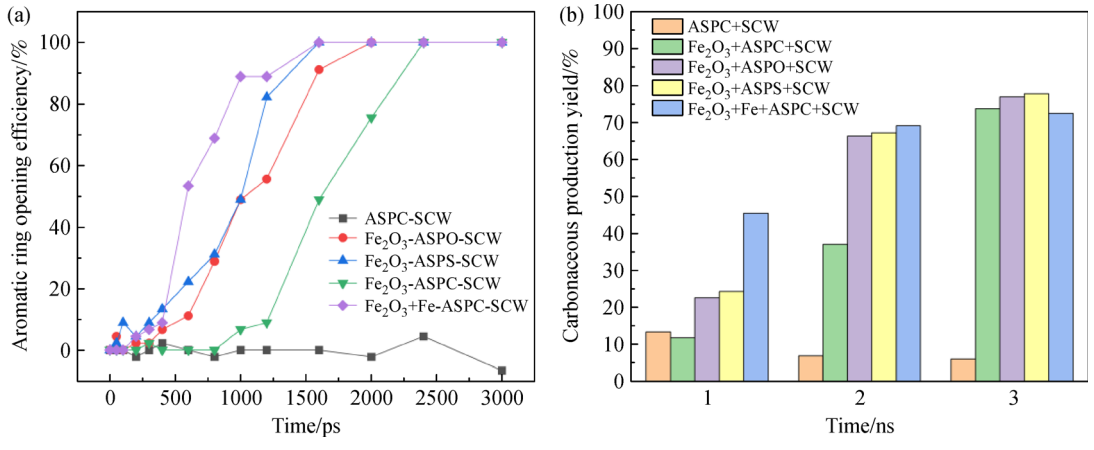

Fig. 6 (a) Time evolution of aromatic ring opening efficiency of asphaltene molecules; (b) carbonaceous production yield of different systems.

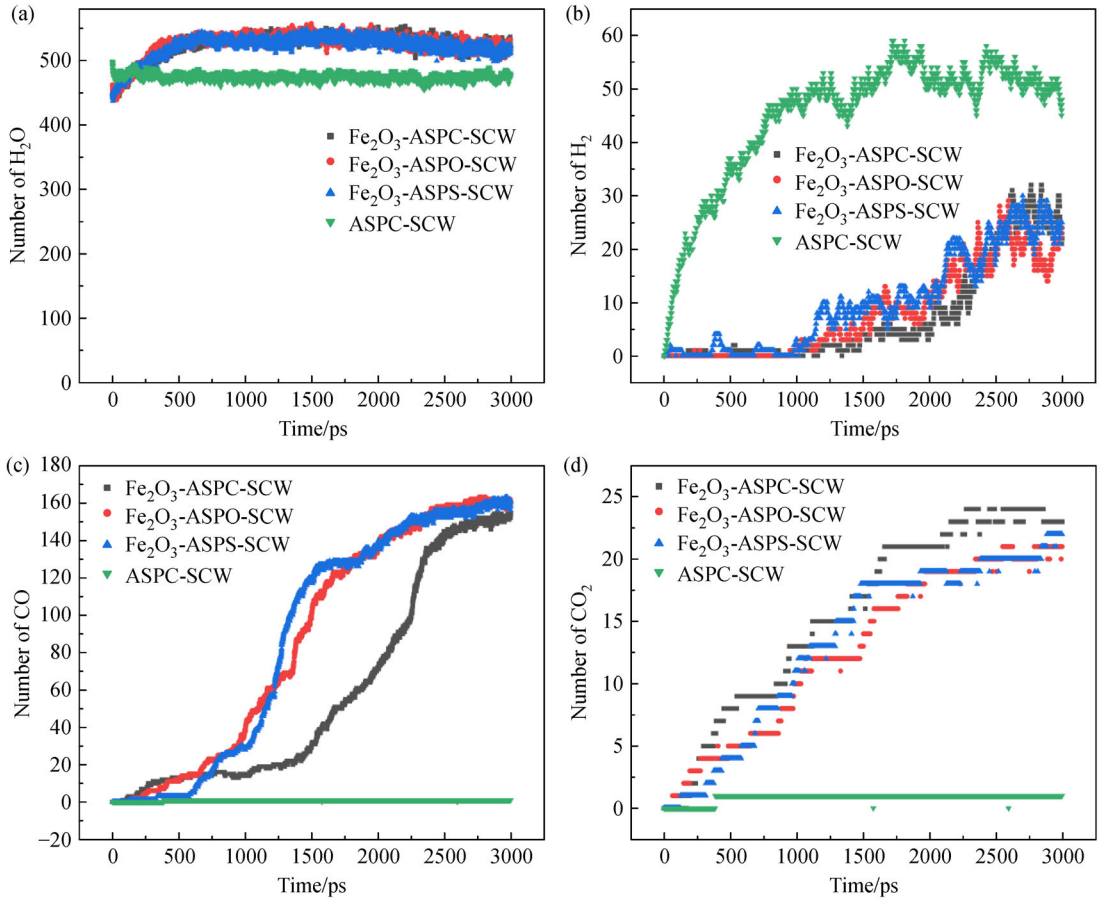

Fig. 7 The number of (a) H_2O, (b) H_2, (c) CO and (d) CO_2 with time in different systems.

generation of CO_2 molecules is much easier in the early stage, while it is prone to generate CO molecules in the later stage shown in Figs. 7(c) and 7(d). On one hand, sufficient lattice oxygen has enough capacity to oxidize small amounts of carbon fragments to form CO_2 in the early stage, on the other hand, large amounts of aromatic ring adsorb on the surface of the catalyst due to the surface lattice oxygen consumed causing that unsaturated coordinated Fe active sites are exposed to the environment, which promotes the degradation of asphaltene molecules to generate CO, and the preference to generate CO in the later stage may be related to the reduction of Fe_2O_3 catalyst with insufficient supplement of lattice oxygen. Interestingly, there is none CH_4 generated in the whole process. In simpler terms, the generation pathway of CH_4 requires the participation of •H radicals which is a serious shortage of supply in these systems, and •H radicals are more likely to bond with lattice oxygen to generate H_2O molecules, even the formation of H_2 is rare. Herein, CH_4 is hard to produce in these simulation systems. Also, CO and CO_2 cannot be seen in the system without Fe_2O_3 catalyst, which is consistent with the aromatic ring opening efficiency shown in Fig. 6(a) owing to the fact that the compounds could not be degraded to form small molecules such as CO.

3.2.3 Generation mechanism of gas products

From the perspective of asphaltene degradation, the carbonaceous production calculated by Eq. (2) could judge the effectiveness of the catalyst, the results are shown in Fig. 6(b). From the perspective of carbonaceous products yield, it has been illustrated that the yield is proportional to the current simulation time expect the system without catalyst and corresponds well to the Fig. 6(a), the earlier the aromatic ring of asphaltene compounds is opened, the higher the carbonaceous products yield is at the corresponding time. Importantly, Fe and Fe_2O_3 catalysts show a synergistic effect on degradation owing to faster aromatic ring opening rate and approximate 45% yield at 1 ns, resulting from that Fe clusters adsorbed on Fe_2O_3 cluster forming more active sites and the lattice oxygen in Fe_2O_3 participates in the degradation process. As a matter of fact, Fe_2O_3 considered as an excellent oxygen carrier has the advantages in the degradation of pollutants, and the carbonaceous production yield can reach almost 80% in the end. Therefore, LOC calculated by Eq. (3) shown in Table 2, a descriptive indicator, has been used to explain that lattice oxygen is involved in the degradation reaction qualitatively. The

value of the LOC of the calculated systems is higher than 100%, it can demonstrate that the lattice oxygen is involved into the whole reaction indeed combining Fig. 7(a) and the calculated values. Herein, the lattice oxygen could be the main contributor of the O source, however, it is undeniable that the O in SCW can also transfer into the catalyst particle and products. Although carbon deposits will inevitably occur, among which are almost carburization to the inside of the crystal. Furthermore, the main pathways of the products are discussed as follows.

Table 2 LOC of different systems

System	Fe_2O_3-ASPC	Fe_2O_3-ASPO	Fe_2O_3-ASPS
Value of LOC	107.62%	107.28%	110.13%

H_2O can be used as a solvent and reactant, meanwhile, it can appear as a product in the SCWG process. The generation pathways of H_2O molecule could be divided into two parts, one is the gradual hydrogenation of O atom shown in Fig. 4, and the other is the rearrangement of HO–C–OH structure to generate H_2O demonstrated in Fig. 2. Figure 2 also exhibits the generation pathway of CO_2, the formed fragment C–O–H bonds with another O to form CO_2 which diffuses into the gas phase immediately. And Fig. 8 shows the typical generation pathways of H_2 and CO. As for H_2, the production pathways of H_2 are related to the source of its hydrogen atoms, combination in H_2O and model compound, and a typical generation pathway is shown in Fig. 8(a). Finally, the C1 fragment formed by cleavage of compounds is adsorbed on the surface of the catalyst, and then bonds with O atom of OH fragment nearby, accompanied with the H atom of OH group captured by Fe active site. Subsequently, the CO would be diffused into the gas phase to generate CO, as can be seen in Fig. 8(b).

3.3 Dispose of heteroatoms and heavy metals

3.3.1 Migration and immobilization of heteroatoms

Figure 9 exhibits the migration path of heteroatoms. As shown in Fig. 9(a), the breakage of C–S bond is considered as the initial step in the conversion of organic sulfur to inorganic sulfur which could remove heteroatom S more easily. Firstly, •OH radical from SCW would be caught by S atom when it gets close enough, forming S–O–H structure. Secondly, the C–S bonds on both sides would be broken under the influence of hydroxyl-terminated in succession. Finally, the crucial intermediate, •HSO radical, is formed which represents the migration of heteroatom S from organic phase into inorganic phase. As a consequence, the final forms of S atoms in the liquid phase are •HSO and $•H_2SO$ radicals. However, the ultimate aim is to separate the inorganic S atom avoiding polluting the environment through the oxidation properties of SCW to oxidize sulfur-containing radicals to SO_4^{2-}, and it could be fixed by adding some chemicals, such as $Ba(OH)_2$. Herein, systems 7 and 8 were conducted to explore the results of recycling solvent and increasing temperature. But unfortunately, heteroatom S atoms could not be oxidized into SO_4^{2-} or SO_3^{2-} in the two simulation systems, perhaps due to the insufficient supplement of O sources. According to the consequence, system 10 was conducted to figure out the reason, thiophene was selected as the model compound is due to the abundant sulfur atoms existing in thiophene. And the results confirm the conjecture that the insufficient supplement of O sources, owing to sulfur existing in large quantities in the form of SO_4^{2-} and SO_3^{2-}. Accordingly, recycling solvent [39] or increasing temperature [40] is effective in fixing heteroatom S.

As for heteroatom O, the migration pathway is shown in Fig. 9(b). The C–O bonds break successively under the effects of SCW, converting into CO, CO_2, H_2O and

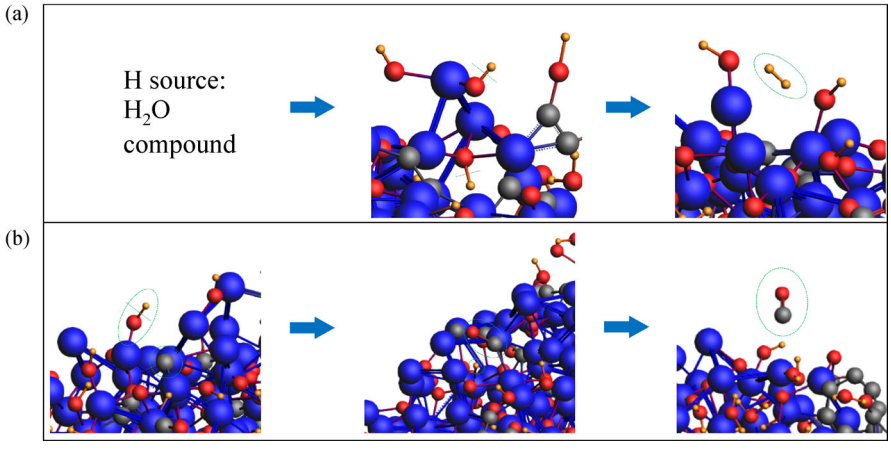

Fig. 8 Generation pathway of (a) H_2 and (b) CO.

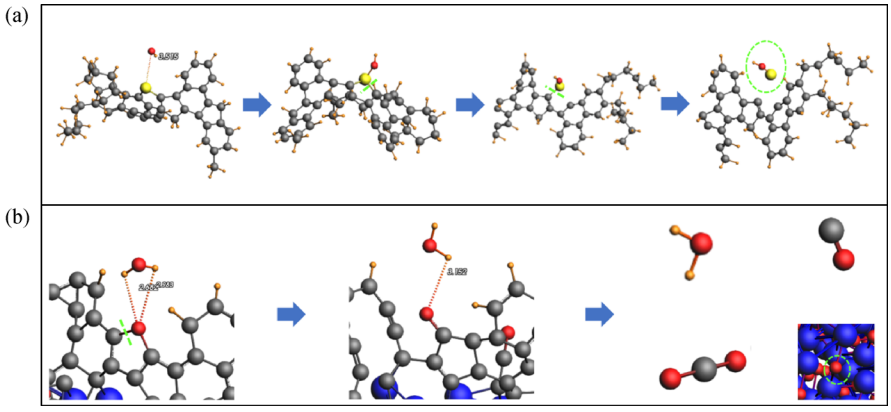

Fig. 9 Migration pathway of (a) S and (b) O atoms in asphaltene.

supplying lattice oxygen. And the migration pathways also demonstrate the difference in the aromatic ring opening efficiency shown in Fig. 6 owing to the different timing of the bonds breaking whether the asphaltene molecules are adsorbed on the surface of the catalyst.

3.3.2 Migration and immobilization of heavy metals

In terms of heavy metals in oil sludge, if it cannot be treated properly, irreversible environmental pollution would be caused due to the leaching of heavy metals. And under hydrothermal conditions, metals adsorbed on the metal oxide substrate tend to agglomerate [41], so as to extent that metal particles in the liquid phase are removed. Herein, system 9 was conducted to investigate the effects of Fe heavy metal to the degradation system. Evidently, it is demonstrated that the agglomeration of Fe and Fe_2O_3 clusters exhibit synergistic effect according to Figs. 6 and 10, and descriptions for Figs. 10(a) and 10(d) are added in supplementary information. Generally speaking, the small

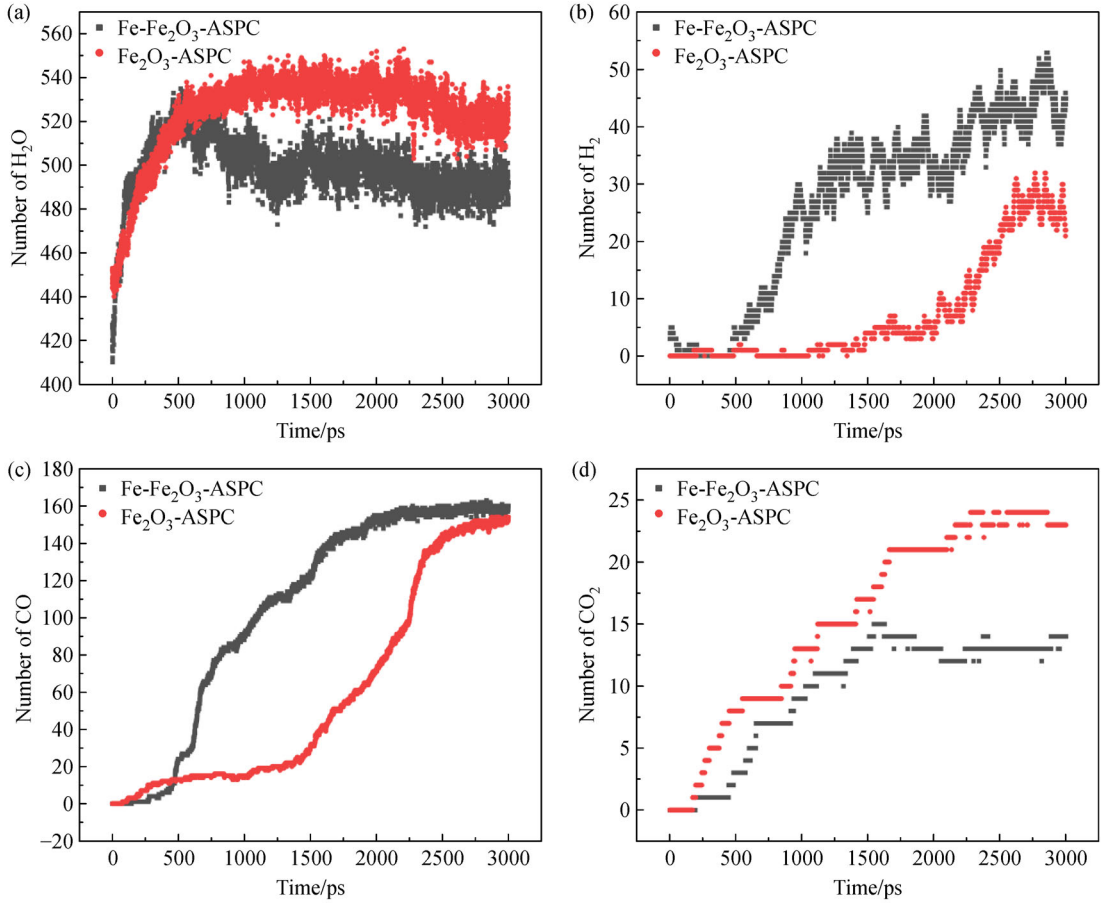

Fig. 10 The number of (a) H_2O, (b) H_2, (c) CO and (d) CO_2 with time in Fe-Fe_2O_3 and Fe_2O_3 systems.

Fe clusters adsorbed on the Fe_2O_3 cluster improve the unsaturated coordination of the catalyst surface which works as the active sites in the initial stage of the process, meanwhile, Fe_2O_3 substrate also works to provide oxygen to degrade compounds. Herein, the agglomerated catalyst improves the degradation efficiency and shortens the reaction time. And it is reported that Ni [42], Zn [43] and Cu [44] have high catalytic performance in SCWG process. Herein, heavy metals can be used in SCWG process to participate in the synergistic reaction, contributing to the reduction in leaching rate of heavy metals.

4 Conclusions

In this work, ReaxFF MD was adopted to investigate the mechanism of Fe_2O_3 catalyst in asphaltene degradation and analyze the formation pathways of products during SCWG process, as well as the migration of heteroatoms and heavy metals. The simulation results demonstrated that the surface lattice oxygen was consumed by small carbon fragments to generate CO and CO_2 contributing to improve to catalytic performance of the cluster due to more unsaturated coordination Fe sites exposed, and then that lattice oxygen combined with •H radicals to from H_2O molecules further improved the catalytic performance. And under the catalysis of Fe_2O_3, the asphaltene molecules underwent a serious ring-opening and rearrangement reactions to form small molecular products, furthermore, the generation pathways were revealed at atomic level. Moreover, the adsorption of •OH radical on S atom caused the breakage of the two C–S bonds in turn, forming the •HSO intermediate, which could be further oxidized through improving the reaction temperature and recycling the solvent in order to fix heteroatom S element easily. Heteroatom O was removed under the effects of SCW. Additionally, heavy metal particles, such as Fe presented in the OS, played a cooperative role with Fe_2O_3 catalyst in accelerating the degradation of asphaltenes, as well as achieving the immobilization of heavy metals.

Acknowledgements This work was supported by the National Natural Science Foundation of China (Grant Nos. 21978210 and U20A20151), Tianjin Natural Science Foundation, China (Grant No. 19JCYBJC20000) and the National Key R&D Program of China (Grant No. 2018YFA0702403). The Gaussian 09 software was supported by the National Supercomputing Center in Shenzhen.

Electronic Supplementary Material Supplementary material is available in the online version of this article at https://dx.doi.org/10.1007/s11705-021-2125-z and is accessible for authorized users.

References

1. Gao N, Li J, Quan C, Tan H. Product property and environmental risk assessment of heavy metals during pyrolysis of oily sludge with fly ash additive. Fuel, 2020, 266: 117090
2. Hamidi Y, Ataei S A, Sarrafi A. A highly efficient method with low energy and water consumption in biodegradation of total petroleum hydrocarbons of oily sludge. Journal of Environmental Management, 2021, 293: 112911
3. Liu J, Zhang Y, Peng K, Zhao X, Xiong Y, Huang X. A review of the interfacial stability mechanism of aging oily sludge: heavy components, inorganic particles, and their synergism. Journal of Hazardous Materials, 2021, 415: 125624
4. Zou H, Liu C, Evrendilek F, He Y, Liu J. Evaluation of reaction mechanisms and emissions of oily sludge and coal co-combustions in O_2/CO_2 and O_2/N_2 atmospheres. Renewable Energy, 2021, 171: 1327–1343
5. Gao N, Li J, Quan C, Wang X, Yang Y. Oily sludge catalytic pyrolysis combined with fine particle removal using a Ni-ceramic membrane. Fuel, 2020, 277: 118134
6. Li Z, Zhou Y, Meng X, Wang S. Harmless and efficient treatment of oily drilling cuttings. Journal of Petroleum Science Engineering, 2021, 202: 108542
7. Gao Y, Ding R, Wu S, Wu Y, Zhang Y, Yang M. Influence of ultrasonic waves on the removal of different oil components from oily sludge. Environmental Technology, 2015, 36(13-16): 1771–1775
8. Chen G, Li J, Li K, Lin F, Tian W, Che L, Yan B, Ma W, Song Y. Nitrogen, sulfur, chlorine containing pollutants releasing characteristics during pyrolysis and combustion of oily sludge. Fuel, 2020, 273: 117772
9. Kruse A, Dahmen N. Water—a magic solvent for biomass conversion. Journal of Supercritical Fluids, 2015, 96: 36–45
10. Okolie J A, Nanda S, Dalai A K, Kozinski J A. Optimization and modeling of process parameters during hydrothermal gasification of biomass model compounds to generate hydrogen-rich gas products. International Journal of Hydrogen Energy, 2020, 45(36): 18275–18288
11. Ding W, Shi J, Wei W, Cao C, Jin H. A molecular dynamics simulation study on solubility behaviors of polycyclic aromatic hydrocarbons in supercritical water/hydrogen environment. International Journal of Hydrogen Energy, 2021, 46(3): 2899–2904
12. Khan M K, Cahyadi H S, Kim S M, Kim J. Efficient oil recovery from highly stable toxic oily sludge using supercritical water. Fuel, 2019, 235: 460–472
13. Adar E, Ince M, Bilgili M S. Supercritical water gasification of sewage sludge by continuous flow tubular reactor: a pilot scale study. Chemical Engineering Journal, 2020, 391: 123499
14. Hantoko D, Antoni, Kanchanatip E, Yan M, Weng Z, Gao Z, Zhong Y. Assessment of sewage sludge gasification in supercritical water for H_2-rich syngas production. Process Safety and Environmental Protection, 2019, 131: 63–72
15. Lin J, Liao Q, Hu Y, Ma R, Cui C, Sun S, Liu X. Effects of process parameters on sulfur migration and H_2S generation during supercritical water gasification of sludge. Journal of Hazardous Materials, 2021, 403: 123678
16. Chen Y, Yi L, Li S, Yin J, Jin H. Catalytic gasification of sewage sludge in near and supercritical water with different catalysts. Chemical Engineering Journal, 2020, 388: 124292
17. Qian L, Wang S, Xu D, Guo Y, Tang X, Wang L. Treatment of

municipal sewage sludge in supercritical water: a review. Water Research, 2016, 89: 118–131
18. Cao C, Xie Y, Mao L, Wei W, Shi J, Jin H. Hydrogen production from supercritical water gasification of soda black liquor with various metal oxides. Renewable Energy, 2020, 157: 24–32
19. Han Y, Wang Y, Ma T, Li W, Zhang J, Zhang M. Mechanistic understanding of Cu-based bimetallic catalysts. Frontiers of Chemical Science and Engineering, 2020, 14(5): 689–748
20. Gao Y, Zhu W, Liu J, Lin P, Zhang J, Huang T, Liu K. Mesoporous sulfur-doped $CoFe_2O_4$ as a new Fenton catalyst for the highly efficient pollutants removal. Applied Catalysis B: Environmental, 2021, 295: 120273
21. van Duin A C T, Dasgupta S, Lorant F, Goddard W A. ReaxFF: a reactive force field for hydrocarbons. Journal of Physical Chemistry A, 2001, 105(41): 9396–9409
22. Han Y, Jiang D, Zhang J, Li W, Gan Z, Gu J. Development, application and challenges of ReaxFF reactive force field in molecular simulations. Frontiers of Chemical Science and Engineering, 2016, 10(1): 16–38
23. Zhang J, Weng X, Han Y, Li W, Cheng J, Gan Z, Gu J. The effect of supercritical water on coal pyrolysis and hydrogen production: a combined ReaxFF and DFT study. Fuel, 2013, 108: 682–690
24. Han Y, Ma T, Chen F, Li W, Zhang J. Supercritical water gasification of naphthalene over iron oxide catalyst: a ReaxFF molecular dynamics study. International Journal of Hydrogen Energy, 2019, 44(57): 30486–30498
25. Zhang J, Gu J, Han Y, Li W, Gan Z, Gu J. Supercritical water oxidation vs supercritical water gasification: which process is better for explosive wastewater treatment? Industrial & Engineering Chemistry Research, 2015, 54(4): 1251–1260
26. Han Y, Chen F, Ma T, Gong H, Al-Shwafy K W A, Li W, Zhang J, Zhang M. Size effect of a Ni nanocatalyst on supercritical water gasification of lignin by reactive molecular dynamics simulations. Industrial & Engineering Chemistry Research, 2019, 58(51): 23014–23024
27. Jiang D, Wang Y, Zhang M, Zhang J, Li W, Han Y. H_2 and CO production through coking wastewater in supercritical water condition: ReaxFF reactive molecular dynamics simulation. International Journal of Hydrogen Energy, 2017, 42(15): 9667–9678
28. Han Y, Ma T, Chen F, Li W, Zhang J. Synergistic mechanism of Ni catalyst and supercritical water during refractory organic wastewater treatment. Industrial & Engineering Chemistry Research, 2019, 58(4): 1535–1547
29. Bai Y, Sui H, Liu X, He L, Li X, Thormann E. Effects of the N, O, and S heteroatoms on the adsorption and desorption of asphaltenes on silica surface: a molecular dynamics simulation. Fuel, 2019, 240: 252–261
30. Schuler B, Meyer G, Pena D, Mullins O C, Gross L. Unraveling the molecular structures of asphaltenes by atomic force microscopy. Journal of the American Chemical Society, 2015, 137(31): 9870–9876
31. Stephens P J, Devlin F J, Chabalowski C F, Frisch M J. Ab initio calculation of vibrational absorption and circular dichroism spectra using density functional force fields. Journal of Chemical Physics, 1994, 98(45): 11623–11627
32. Krishnan R, Binkley J S, Seeger R, Pople J A. Self-consistent molecular orbital methods. XX. A basis set for correlated wave functions. Journal of Chemical Physics, 1980, 72(1): 650–654
33. Shin Y K, Kwak H, Vasenkov A V, Sengupta D, van Duin A C T. Development of a ReaxFF reactive force field for Fe/Cr/O/S and application to oxidation of butane over a pyrite-covered Cr_2O_3 catalyst. ACS Catalysis, 2015, 5(12): 7226–7236
34. Hu Y, Qi L, Rao K T V, Zhao B, Li H, Zeng Y, Xu C. Supercritical water gasification of biocrude oil from low-temperature liquefaction of algal lipid extraction residue. Fuel, 2020, 276: 118017
35. Sorensen M R, Voter A F. Temperature-accelerated dynamics for simulations of infrequent events. Journal of Chemical Physics, 2000, 112(21): 9599–9606
36. Wang X, Xue X, Zhang C. Early events of the carburization of Fe nanoparticles in ethylene pyrolysis: reactive force field molecular dynamics simulations. Journal of Physical Chemistry C, 2018, 122(20): 10835–10845
37. Bentria E T, Akande S O, Becquart C S, Mousseau N, Bouhali O, El-Mellouhi F. Capturing the iron carburization mechanisms from the surface to bulk. Journal of Physical Chemistry C, 2020, 124(52): 28569–28579
38. Liu X, Wen X, Hoffmann R. Surface activation of transition metal nanoparticles for heterogeneous catalysis: what we can learn from molecular dynamics. ACS Catalysis, 2018, 8(4): 3365–3375
39. Chen H, He Z, Zhang B, Feng H, Kandasamy S, Wang B. Effects of the aqueous phase recycling on bio-oil yield in hydrothermal liquefaction of spirulina platensis, α-cellulose, and lignin. Energy, 2019, 179: 1103–1113
40. Meng N, Jiang D, Liu Y, Gao Z, Cao Y, Zhang J, Gu J, Han Y. Sulfur transformation in coal during supercritical water gasification. Fuel, 2016, 186: 394–404
41. Dasireddy V D B C, Likozar B. Direct methanol production from mixed methane/H_2O/N_2O feedstocks over Cu-Fe/Al_2O_3 catalysts. Fuel, 2021, 301: 121084
42. Kou J, Yi L, Li G, Cheng K, Wang R, Zhang D, Jin H, Guo L. Structural effect of ZrO_2 on supported Ni-based catalysts for supercritical water gasification of oil-containing wastewater. International Journal of Hydrogen Energy, 2021, 46(24): 12874–12885
43. Mastuli M S, Kamarulzaman N, Kasim M F, Mahat A M, Matsumura Y, Taufiq-Yap Y H. Catalytic supercritical water gasification of oil palm frond biomass using nanosized MgO doped Zn catalysts. Journal of Supercritical Fluids, 2019, 154: 104610
44. Samiee-Zafarghandi R, Hadi A, Karimi-Sabet J. Graphene-supported metal nanoparticles as novel catalysts for syngas production using supercritical water gasification of microalgae. Biomass and Bioenergy, 2019, 121: 13–21